Observational constraints on self-accelerating cosmology

Roy Maartens and Elisabetta Majerotto

Institute of Cosmology & Gravitation, University of Portsmouth, Portsmouth PO1 2EG, UK

(Dated: February 5, 2008)

The DGP brane-world model provides a simple alternative to the standard LCDM cosmology, with the same number of parameters. There is no dark energy – the late universe self-accelerates due to an infrared modification of gravity. We compute the joint constraints on the DGP model from supernovae, the cosmic microwave background shift parameter, and the baryon oscillation peak in the SDSS luminous red galaxy sample. Flat DGP models are within the joint 2 sigma contour, but the LCDM model provides a significantly better fit to the data. These tests are based on the background dynamics of the DGP model, and we comment on further tests that involve structure formation.

PACS numbers: 95.36.+x, 98.80.-k, 98.80.Es

1. THE DARK ENERGY PROBLEM

The acceleration of the late-time universe, as implied by observations of supernovae, cosmic microwave background anisotropies and the large-scale structure, poses one of the deepest theoretical problems facing cosmology [1]. Within the framework of general relativity, the acceleration originates from a dark energy field (or effective dark energy) with negative pressure ($w \equiv p/\rho < -\frac{1}{3}$), such as vacuum energy ($w = -1$) or a slow-rolling scalar field ("quintessence", $w > -1$). So far, none of the available models has a natural explanation.

For the simplest option of vacuum energy, i.e., the LCDM model, the incredibly small value of the cosmological constant

$$\rho_{\Lambda,\text{obs}} = \frac{\Lambda}{8\pi G} \sim H_0^2 M_P^2 \sim (10^{-3} \text{ eV})^4 \,, \qquad (1)$$

$$\rho_{\Lambda,\text{theory}} \sim M_{\text{fundamental}}^4 > (1 \text{ TeV})^4 \gg \rho_{\Lambda,\text{obs}} \,, \quad (2)$$

cannot be explained by current particle physics. In addition, the value needs to be fine-tuned,

$$\Omega_\Lambda \sim \Omega_{\text{m}} \,, \qquad (3)$$

which also has no natural explanation. Quintessence models attempt to address the fine-tuning problem, but do not produce a natural solution – and also cannot address the problem of how Λ is set exactly to 0.

Alternatively, it is possible that there is no dark energy, but instead an infrared modification of general relativity, i.e., on very large scales, $r \gtrsim H_0^{-1}$, that accounts for late-time acceleration. (Note that this does not remove the problem of explaining why the vacuum energy does not gravitate.) Schematically, we are modifying the geometric side of the field equations,

$$G_{\mu\nu} + G_{\mu\nu}^{\text{dark}} = 8\pi G T_{\mu\nu} \,, \qquad (4)$$

rather than the matter side,

$$G_{\mu\nu} = 8\pi G \left(T_{\mu\nu} + T_{\mu\nu}^{\text{dark}} \right) \,, \qquad (5)$$

as in general relativity. It is important that the modification is covariant and incorporates deviations from homogeneity and isotropy, so that one can compute not only the background dynamics, but also the perturbations.

2. DGP MODIFIED GRAVITY

One of the simplest covariant modified-gravity models is based on the Dvali-Gabadadze-Porrati (DGP) brane-world model, as generalized to cosmology by Deffayet [2]. (It is worth noting that the original DGP model with a Minkowski brane was not introduced to explain acceleration – the generalization to a Friedman brane was subsequently found to be self-accelerating.) In this model, gravity leaks off the 4-dimensional brane universe into the 5-dimensional bulk spacetime at large scales. At small scales, gravity is effectively bound to the brane and 4D gravity is recovered to a good approximation, via the lightest modes of the 5D graviton – effectively via an ultralight metastable graviton in the 4D universe. The transition from 4D to 5D behaviour is governed by a crossover scale r_c; the weak-field gravitational potential behaves as r^{-1} for $r \ll r_c$ and as r^{-2} for $r \gg r_c$.

The energy conservation equation remains the same as in general relativity, but the Friedman equation is modified:

$$\dot{\rho} + 3H(\rho + p) = 0 \,, \qquad (6)$$

$$H^2 + \frac{K}{a^2} - \frac{1}{r_c}\sqrt{H^2 + \frac{K}{a^2}} = \frac{8\pi G}{3}\rho \,. \qquad (7)$$

These equations imply (for the CDM case $p = 0$)

$$\dot{H} - \frac{K}{a^2} = -4\pi G\rho \left[1 + \frac{1}{\sqrt{1 + 32\pi Gr_c^2\rho/3}} \right] \,. \qquad (8)$$

Equation (7) shows that at early times, when $H^2 + K/a^2 \gg r_c^{-2}$, the general relativistic Friedman equation is recovered. By contrast, at late times in a CDM uni-

verse, with $\rho \propto a^{-3} \to 0$, we have

$$H \to H_\infty = \frac{1}{r_c} \,. \qquad (9)$$

Gravity leakage at late times initiates acceleration – not due to any negative pressure field, but due to the weakening of gravity on the brane. Since $H_0 > H_\infty$, in order to achieve self-acceleration at late times, we require

$$r_c \gtrsim H_0^{-1} \,, \qquad (10)$$

and this is confirmed by fitting observations, as discussed below.

In dimensionless form, the modified Friedman equation (7) is

$$\frac{H(z)^2}{H_0^2} = \left[\sqrt{\Omega_{\mathrm{m}}(1+z)^3 + \Omega_{r_c}} + \sqrt{\Omega_{r_c}} \right]^2 + \Omega_K(1+z)^2 \,, \qquad (11)$$

where

$$\Omega_K = 1 - \Omega_{\mathrm{m}} - 2\sqrt{\Omega_{r_c}}\left(\sqrt{\Omega_{r_c}} + \sqrt{\Omega_{r_c} + \Omega_{\mathrm{m}}}\right), (12)$$

$$\Omega_{r_c} = \frac{1}{4H_0^2 r_c^2} \,. \qquad (13)$$

From Eq. (8), the dimensionless acceleration is

$$\frac{1}{H_0^2}\frac{\ddot{a}}{a} = \left(\sqrt{\Omega_{\mathrm{m}}(1+z)^3 + \Omega_{r_c}} + \sqrt{\Omega_{r_c}}\right)\left[\sqrt{\Omega_{r_c}} + \frac{2\Omega_{r_c} - \Omega_{\mathrm{m}}(1+z)^3}{2\sqrt{\Omega_{\mathrm{m}}(1+z)^3 + \Omega_{r_c}}}\right], \qquad (14)$$

so that the redshift when acceleration starts is given by

$$1 + z_a = 2\left(\frac{\Omega_{r_c}}{\Omega_{\mathrm{m}}}\right)^{1/3} \,. \qquad (15)$$

The $(\Omega_{r_c}, \Omega_{\mathrm{m}})$ plane is illustrated in Fig. 1. This shows the flat model curve [from Eq. (12)],

$$\Omega_{r_c} = \frac{1}{4}(1 - \Omega_{\mathrm{m}})^2, \qquad (16)$$

and the present-time zero-acceleration curve [from Eq. (15)],

$$\Omega_{r_c} = \frac{\Omega_{\mathrm{m}}}{8} \,. \qquad (17)$$

By checking for real roots $z > 0$ of the equation $H(z) = 0$, given by Eq. (11) with radiation included, we also find the region of the plane containing bouncing models, i.e., models that are currently expanding but were collapsing in the past.

The modified Friedman equation in DGP may reinterpreted from a standard viewpoint. We define the effective dark energy density $\rho_{\mathrm{eff}} \equiv 3H/8\pi G r_c$. Then the effective
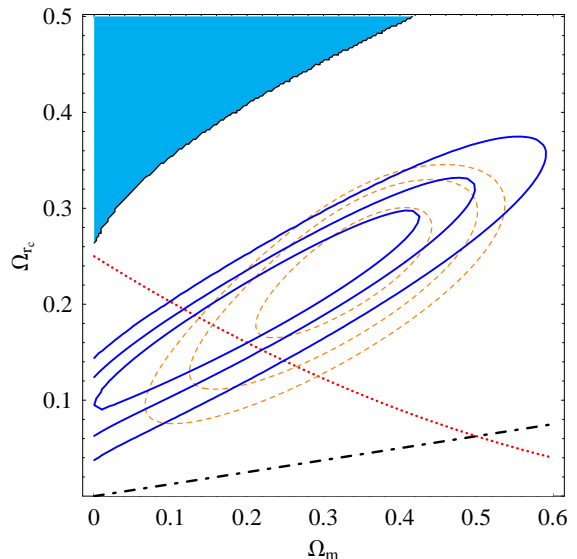

FIG. 1: The parameter space for DGP models. The dotted (red) curve is the flat case, with closed models above and open models below; the dot-dashed (black) curve demarcates models that are currently accelerating (above) from those decelerating (below); the shaded (blue) region contains expanding models that bounce in the past, i.e. do not have a big bang; the likelihood contours are fits to the SNe Gold data [dashed (brown)] and Legacy data [solid (blue)].

dark energy equation of state $w_{\mathrm{eff}} \equiv p_{\mathrm{eff}}/\rho_{\mathrm{eff}}$ is given by $\dot{\rho}_{\mathrm{eff}} + 3H(1 + w_{\mathrm{eff}})\rho_{\mathrm{eff}} = 0$. Thus ρ_{eff} and w_{eff} give a standard general relativistic interpretation of DGP expansion history, i.e., they describe the equivalent general relativity dark energy model. For the flat case, $\Omega_K = 0$, we find

$$w_{\mathrm{eff}}(z) = \frac{\Omega_{\mathrm{m}} - 1 - \sqrt{(1 - \Omega_{\mathrm{m}})^2 + 4\Omega_{\mathrm{m}}(1+z)^3}}{2\sqrt{(1 - \Omega_{\mathrm{m}})^2 + 4\Omega_{\mathrm{m}}(1+z)^3}} \,, \qquad (18)$$

which implies

$$w_{\mathrm{eff}}(0) = -\frac{1}{1 + \Omega_{\mathrm{m}}} \,. \qquad (19)$$

The DGP and LCDM models have the same number of parameters, with r_c substituting for Λ. (Neither model provides a natural solution to the late-acceleration problem – both Λ and r_c must be fine-tuned to match observations.) The DGP cosmology therefore gives a very useful framework for comparing the LCDM general relativistic cosmology to a modified gravity alternative. Does the DGP model pass the observational tests? The next section considers this question.

3. OBSERVATIONAL CONSTRAINTS ON DGP

The fundamental test of the background dynamics of a cosmological model is the SNe magnitude-redshift test,
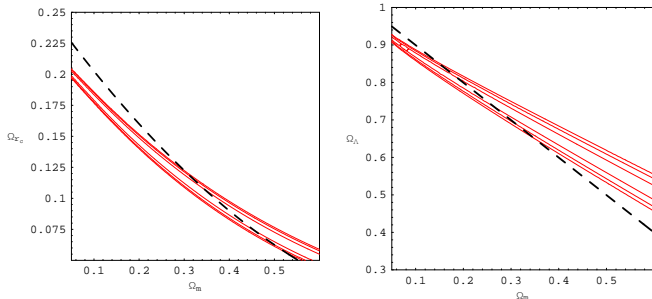
FIG. 2: Likelihood contours for the CMB shift parameter S in DGP (left) and LCDM (right).

based on the luminosity distance,

$$
d_L = \frac{(1+z)}{H_0\sqrt{|\Omega_K|}} \mathcal{F}\left(\sqrt{|\Omega_K|}\int_0^z \frac{dz'}{H(z')/H_0}\right), \quad (20)
$$

where

$$
\mathcal{F}(x) \equiv (x, \sin x, \sinh x) \text{ for } K = (0, 1, -1). \quad (21)
$$

The 68, 95 and 99% likelihood contours from fits to the SNe data [3, 4] are shown in the DGP parameter plane in Fig. 1.

The luminosity distance is determined purely by the modified Friedman equation (11), and there is a general relativistic dark energy model that can exactly mimic the DGP luminosity distance. This equivalent model has dark energy equation of state equal to the DGP effective equation of state w_{eff}, as given in Eq. (18) for the flat case. Of course, there is no physical justification for the equivalent general relativistic model, whereas the DGP model has a clear physical motivation. Nevertheless, tests based on the Hubble rate $H(z)$ cannot distinguish the DGP from a GR dark energy model. Further tests are needed to discriminate DGP from general relativistic models. The CMB anisotropies and matter power spectrum provide in principle suitable discriminatory tests. These tests require a detailed understanding of the evolution of density perturbations in the DGP model. Unfortunately the problem is highly complicated and not yet solved, essentially since density perturbations are coupled to perturbations in the 5D gravitational field [5].

Previous results on the CMB anisotropies and structure formation in DGP [6] provide valuable strategies for testing DGP and discriminating it from general relativistic models. However, these results are based on neglecting the 5D perturbations, which effectively imposes an inconsistency, leading to a violation of the 4D Bianchi identity, as explained by Koyama and Maartens [5]. On sub-Hubble scales, linear density perturbations in the DGP model have been computed in a way that satisfies the 5D equations [5], and this result confirms and generalizes the results of Lue and Starkman [7]. Further work

is needed to quantify the corrections to general relativistic perturbations on scales near and above the Hubble radius.

Until the problem of cosmological perturbations in DGP is solved, we must turn to other observations, independent of the SNe redshifts, that rely on the background model and do not rely (or rely only weakly) on the density perturbations.

CMB shift

The CMB shift parameter

$$
S = \sqrt{\Omega_{\text{m}}} H_0 \frac{d_L(z_r)}{(1+z_r)}, \quad (22)
$$

relates the angular scale of the first acoustic peak to the angular diameter distance to last scattering and the physical scale of the sound horizon. It is effectively model-independent and insensitive to perturbations, and may be used to constrain the background dynamics of models, such as quintessence models [8]. Wang and Mukherjee [9] have used the WMAP 3-year data [10] to derive

$$
S = 1.70 \pm 0.03, \quad (23)
$$

with $z_r = 1090$. The likelihood contours for S in the DGP and LCDM cases are shown in Fig. 2. Note that the DGP contours are more in the open-model region for $\Omega_{\text{m}} \lesssim 0.4$ than the LCDM contours.

Baryon oscillations

Fairbairn and Goobar [11] used the baryon acoustic oscillation peak recently detected in the SDSS luminous red galaxies (LRGs) [12] as an independent test of the DGP. The correlation function for SDSS LRGs shows a peak at a scale $\sim 100h^{-1}$ Mpc, corresponding to the first acoustic peak at recombination (determined by the sound horizon). The observed scale effectively constrains the quantity [12]

$$
A = \sqrt{\Omega_{\text{m}}} \left[\frac{H_0^3 \, d_L^2(z_1)}{H_1 z_1^2 (1+z_1)^2}\right]^{1/3}, \quad (24)
$$

and Eisenstein et al. find that [12]

$$
A = 0.469 \pm 0.017, \quad (25)
$$

where $z_1 = 0.35$ is the typical LRG redshift. (Following Ref. [11], we have suppressed a weak dependence of A on the spectral tilt.)

We should point out that there is a level of uncertainty in the use of the BO measure A. The BO data are analyzed via a fiducial LCDM model, with a single scaling relation used to make a best fit, and a compression of the data to a constraint at a single redshift [12].
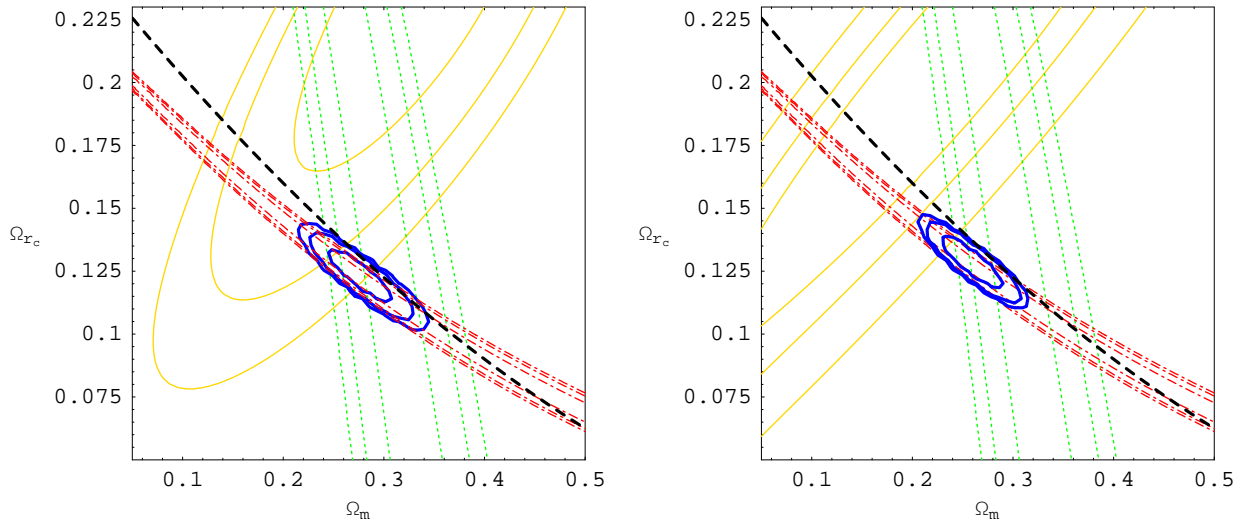
FIG. 3: Joint constraints [solid thick (blue)] on DGP models from the SNe data [solid thin (yellow)], the BO measure A [dotted (green)] and the CMB shift parameter S [dot-dashed (red)]. The left plot uses SNe Gold data, the right plot uses SNLS data. The thick dashed (black) line represents the flat models, $\Omega_K = 0$.
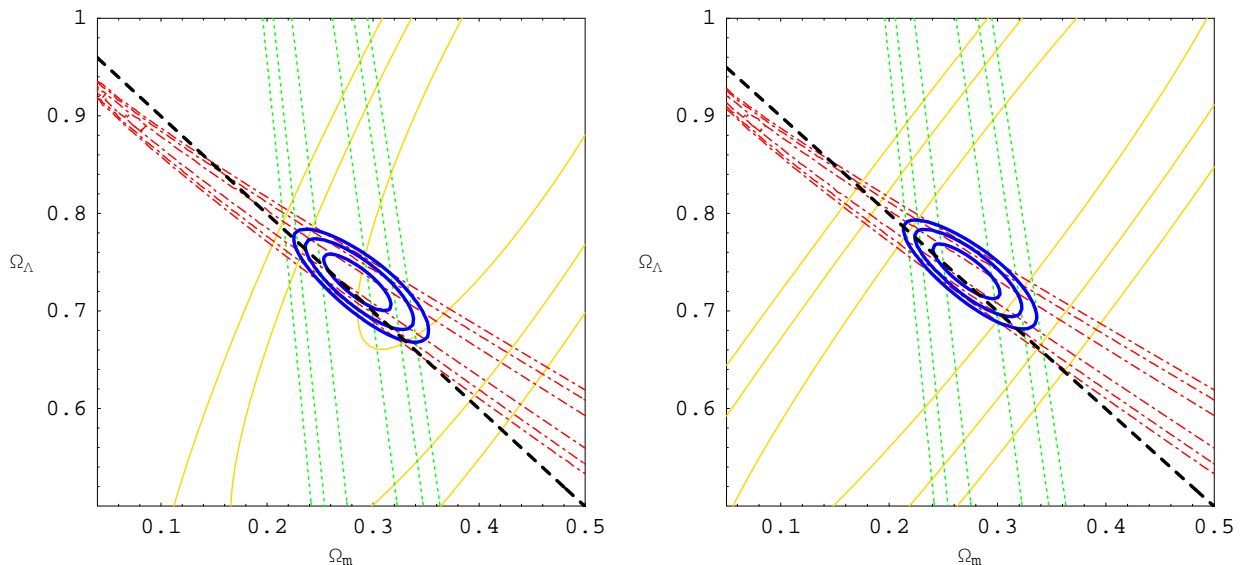

FIG. 4: As in Fig. 3, but for LCDM.

Within the LCDM class of models, this approximation is accurate to within a few percent [12] (less than current errors in the determination of $\Omega_{\rm m}$). As pointed out by Dick et al. [13], this single-redshift feature, which may be robust for LCDM and constant-w models, could introduce significant errors for models with nonconstant w. The DGP has an effective nonconstant w, although over the SDSS LRG redshift range ($0.16 \leq z \leq 0.47$)

the variation is small. It is not clear whether the errors introduced in fitting DGP models are at the acceptable level of a few percent. It is effectively implicitly assumed that this is the case in Refs. [11, 14, 15]. This may be a reasonable assumption, since the DGP comoving luminosity distance is close to LCDM in the redshift range for the LRGs [5]. Ultimately, the BO data should be re-analyzed without assuming a fiducial LCDM model and

without compression to a single redshift, so as to be a more reliable constraint on alternatives to LCDM.

Another issue is the extent to which the BO constraint relies on the LCDM matter power spectrum. The DGP corrections to the shape of the matter power spectrum at last scattering on scales around the first acoustic peak scale are small, although there may be some scale-dependence in the corrections [16].

Fairbairn and Goobar showed that the joint constraints from SNe (Legacy) data and the BO measure A ruled out a flat DGP model at 3σ. Alam and Sahni [14] used the Gold SNe data with the BO measure A and showed that the flat DGP model is marginally allowed at 2σ. (See also Refs. [15].) A conservative conclusion from these results is that the SNe-BO constraints exclude flat DGP models at 2σ, unlike the case of LCDM models, where flat models are within the joint 1σ contour [4].

However, this negative conclusion is over-turned when we include the CMB constraint from S.

Combined SNe-CMB-BO constraints

The effect of the CMB shift S is to pull the best-fit model down from the closed region towards the flat curve. This is clearly illustrated in Fig. 3: without the shift constraint, the joint SNe-BO best-fit would be well above the flat model curve, as found by Fairbairn and Goobar [11].

The corresponding constraints for the LCDM model are shown in Fig. 4, and are consistent with the results of Ichikawa and Takahashi [17]. For LCDM, the SNe-BO constraints already allow a flat model at 1σ, and the effect of the shift parameter is simply to narrow and rotate the contours. It is clear from Figs. 3 and 4 that there is some tension between the data and DGP, which is not the case for LCDM.

4. CONCLUSIONS

The combination of three independent observational constraints – SNe, CMB shift parameter, baryon oscillations – is a powerful way to test the background dynamics of a cosmological model. It has been used for quintessence models by Ichikawa and Takahashi [17] and for an $f(R)$ modified gravity model by Amarzguioui et al. [18]. We applied this triple joint constraint to the DGP case, using both the Gold and the Legacy data, and showed that flat DGP models are within the 2σ joint contour. We note that the best-fit DGP model is slightly open, as opposed to the slightly closed nature of the best-fit LCDM model.

Although flat DGP and LCDM models are both within the 2σ contour, it is clear from Figs. 3 and 4 that LCDM fits the data more easily. A quantitative measure of this is via the χ^2 values for the best-fit models in the two cases, as shown in Tables I (Gold SNe data) and II (Legacy SNe data). The tension between the data and the DGP

is signalled by the rather large value of $w_{\text{eff}}(0)$: using $\Omega_{\text{m}} \approx 0.26$ from Tables I and II, Eq. (19) gives

$$w_{\text{eff}}(0) \approx -0.8 . \qquad (26)$$

	best-fit acceleration parameter	best-fit density parameter	best-fit curvature parameter	χ^2 value
DGP	$\Omega_{r_c} = 0.125$	$\Omega_{\text{m}} = 0.270$	$\Omega_K = +0.0278$	185.0
LCDM	$\Omega_\Lambda = 0.730$	$\Omega_{\text{m}} = 0.285$	$\Omega_K = -0.0150$	177.8

TABLE I: Best-fit parameters from SNe (Gold)-CMB shift-BO constraints, and χ^2 values, for the DGP and LCDM models.

	best-fit acceleration parameter	best-fit density parameter	best-fit curvature parameter	χ^2 value
DGP	$\Omega_{r_c} = 0.130$	$\Omega_{\text{m}} = 0.255$	$\Omega_K = +0.0300$	128.8
LCDM	$\Omega_\Lambda = 0.740$	$\Omega_{\text{m}} = 0.270$	$\Omega_K = -0.0100$	113.6

TABLE II: As in Table I, for the Legacy SNe data.

For the Gold data, LCDM reduces the χ^2 by 7, whereas the Legacy data gives an even larger reduction of 15. LCDM provides a significantly better fit to SNe-CMB shift-BO observations than DGP, especially for the Legacy SNe data.

The χ^2 per degree of freedom provides a comparison of the goodness of fit across the two SNe data sets:

$$\left(\chi^2/\text{dof}\right)_{\text{DGP}} = \begin{cases} 1.179 & \text{Gold} \\ 1.120 & \text{Legacy} \end{cases}$$

$$\left(\chi^2/\text{dof}\right)_{\text{LCDM}} = \begin{cases} 1.132 & \text{Gold} \\ 0.988 & \text{Legacy} \end{cases}$$

The Legacy data leads to a better fit for both DGP and LCDM.

One qualification to our results is that we have not shown the reliability of the BO measure A as a clean test of the background dynamics for DGP (this also applies to previous applications of the BO constraint to DGP models [11, 14, 15]). The BO measure A is tailored to the LCDM model, as explained above. Although we may expect that only small corrections are involved, it is not clear whether this introduces an artificial bias against the DGP model. This is a nontrivial problem to resolve, and further work is needed.

At a more fundamental level, the DGP needs to be tested against the data on CMB anisotropies and the matter power spectrum, and these tests provide also the

means to discriminate DGP from the equivalent general relativistic dark energy model. However, as explained above, theses tests cannot yet be carried out, since the analysis of the density perturbations in DGP has not yet been sufficiently developed [5]. We should also note that there is a ghost at the linear perturbative level in the asymptotic de Sitter state of the self-accelerating DGP cosmology [19]. Classically, this ghost is not a problem, but it does render the quantum vacuum unstable, and we effectively assume that an ultraviolet completion of the DGP model may be found that cures the ghost instability in the quantum vacuum.

[1] For recent discussions, see, e.g.,
L. Perivolaropoulos, arXiv:astro-ph/0601014;
S. Nojiri and S. D. Odintsov, arXiv:hep-th/0601213;
T. Padmanabhan, arXiv:astro-ph/0603114;
E. J. Copeland, M. Sami and S. Tsujikawa, arXiv:hep-th/0603057;
N. Straumann, arXiv:hep-ph/0604231;
S. Bludman, arXiv:astro-ph/0605198;
J. P. Uzan, arXiv:astro-ph/0605313.

[2] G. R. Dvali, G. Gabadadze and M. Porrati, Phys. Lett. B **484**, 112 (2000) [arXiv:hep-th/0002190];
C. Deffayet, Phys. Lett. B **502**, 199 (2001) [arXiv:hep-th/0010186].

[3] A. G. Riess *et al.* [Supernova Search Team Collaboration], Astrophys. J. **607**, 665 (2004) [arXiv:astro-ph/0402512].

[4] P. Astier *et al.*, Astron. Astrophys. **447**, 31 (2006) [arXiv:astro-ph/0510447].

[5] K. Koyama and R. Maartens, JCAP **0610**, 016 (2006) [arXiv:astro-ph/0511634].

[6] C. Deffayet, S. J. Landau, J. Raux, M. Zaldarriaga and P. Astier, Phys. Rev. D **66**, 024019 (2002) [arXiv:astro-ph/0201164];
Y. S. Song, Phys. Rev. D **71**, 024026 (2005) [arXiv:astro-ph/0407489];
L. Knox, Y. S. Song and J. A. Tyson, arXiv:astro-ph/0503644;
I. Sawicki and S. M. Carroll, arXiv:astro-ph/0510364;
M. Ishak, A. Upadhye and D. N. Spergel, arXiv:astro-ph/0507184.

[7] A. Lue and G. Starkman, Phys. Rev. D **67**, 064002 (2003) [arXiv:astro-ph/0212083];
A. Lue, R. Scoccimarro and G. D. Starkman, Phys. Rev. D **69**, 124015 (2004) [arXiv:astro-ph/0401515];
A. Lue, Phys. Rept. **423**, 1 (2006) [arXiv:astro-ph/0510068].

[8] See, e.g., Y. Wang and P. Mukherjee, Astrophys. J. **606**, 654 (2004) [arXiv:astro-ph/0312192];
Y. Wang and M. Tegmark, Phys. Rev. Lett. **92**, 241302 (2004) [arXiv:astro-ph/0403292];
V. F. Cardone, A. Troisi and S. Capozziello, Phys. Rev. D **72**, 043501 (2005) [arXiv:astro-ph/0506371].

[9] Y. Wang and P. Mukherjee, arXiv:astro-ph/0604051.

[10] D. N. Spergel *et al.*, arXiv:astro-ph/0603449.

[11] M. Fairbairn and A. Goobar, arXiv:astro-ph/0511029.

[12] D. J. Eisenstein *et al.*, Astrophys. J. **633**, 560 (2005) [arXiv:astro-ph/0501171].

[13] J. Dick, L. Knox and M. Chu, arXiv:astro-ph/0603247.

[14] U. Alam and V. Sahni, Phys. Rev. D **73**, 084024 (2006) [arXiv:astro-ph/0511473].

[15] Z. K. Guo, Z. H. Zhu, J. S. Alcaniz and Y. Z. Zhang, arXiv:astro-ph/0603632;
M. C. Bento, O. Bertolami, M. J. Reboucas and N. M. C. Santos, arXiv:astro-ph/0603848;
K. Yamamoto, B. A. Bassett, R. C. Nichol and Y. Suto, arXiv:astro-ph/0605278.

[16] K. Koyama, private communication.

[17] K. Ichikawa and T. Takahashi, Phys. Rev. D **73**, 083526 (2006) [arXiv:astro-ph/0511821].

[18] M. Amarzguioui, O. Elgaroy, D. F. Mota and T. Multamaki, arXiv:astro-ph/0510519.

[19] D. Gorbunov, K. Koyama and S. Sibiryakov, Phys. Rev. D **73**, 044016 (2006) [arXiv:hep-th/0512097];
C. Charmousis, R. Gregory, N. Kaloper and A. Padilla, arXiv:hep-th/0604086.